

Research Article

Takashi Sato*, Akiko Yamada and Takeshi Suto

Focus tolerance influenced by source size in Talbot lithography

DOI 10.1515/aot-2015-0022

Received March 14, 2015; accepted May 20, 2015; previously published online June 16, 2015

Abstract: Using a simulation, we investigate the effects of the light source size and derive an effective method for suppression of the subfringes that appear in ArF Talbot lithography, which has been proposed for submicron pattern transfer applications. The appearance of the subfringes, which were caused by interference, was related to the size of the light source. If an appropriate light source size is chosen, then, a large process window can be obtained. Guidelines for source size selection are given.

Keywords: interference; light source size; lithography; process window; Talbot effect.

OCIS code: 110.5220 Photolithography.

1 Introduction

Gratings have many interesting behavioral aspects. The structure of a grating is simple, but many papers continue to be published about grating structures today. In the 1830s, H.F. Talbot reported a phenomenon, which, according to Talbot, was ‘any more than ever-changing figures of the kaleidoscope’ when he viewed ‘the light which had passed through this grating with a lens of considerable magnifying power’ [1]. He was viewing a grating made by Fraunhofer. Forty-five years after Talbot’s observation, Lord Rayleigh explained this effect mathematically

*Corresponding author: Takashi Sato, Center for Semiconductor Research and Development, Toshiba Corporation 1, Komukai Toshiba-cho, Saiwai-ku, Kawasaki, Kanagawa 212-8583, Japan, e-mail: ta.sato@toshiba.co.jp

Akiko Yamada and Takeshi Suto: Center for Semiconductor Research and Development, Toshiba Corporation 1, Komukai Toshiba-cho, Saiwai-ku, Kawasaki, Kanagawa 212-8583, Japan

www.degruyter.com/aot

© 2015 THOSS Media and De Gruyter

[2]. Today, this effect is known as the Talbot effect: a self-imaging phenomenon that enables lensless imaging. There are many applications of this phenomenon, and a review paper that describes the principle and recent studies of the phenomenon is available [3].

We would now like to consider semiconductor lithography. The most advanced lithography tools use sophisticated multimirror optics with an extreme ultraviolet source or an immersion lens with an ArF excimer laser source [4, 5]. At the same time, reduction of the production costs for semiconductor chips continues to act as an incentive for further development of lithographic technology [6], and from this viewpoint, proximity lithography is a strong candidate to provide a cost-effective method because it requires no projection optics, although it does have limitations in terms of resolving power. Several ideas have been proposed to overcome these limitations [7], and Talbot lithography is expected to demonstrate good performance levels [8–16]. Because Talbot lithography involves a type of interference patterning, it generates interference fringes, which are called the Talbot carpet. If the pattern pitch is close to the wavelength of the light source, then a simple repeated pattern is obtained [8, 10]. However, if the pattern pitch is much larger than the source wavelength, the transferred pattern is not so simple [17]. These fringes could yield unwanted results for the transferred pattern. Therefore, suppression of the unwanted fringes is likely to be an issue in the development of Talbot lithography. Here we focus on submicron pattern transfer using a 193-nm light source and discuss the appearance of the unwanted fringes. These subpattern fringes are simulated and are shown to be a pitch dependency of the Talbot effect. We then discuss the effects of the size of the light source and derive an effective method to suppress the fringes.

2 Simulation

Our discussion of the Talbot effect begins here on the basis of an optical simulation. The Talbot effect is known

to be dependent on the polarization when the grating pitch is close to the wavelength of the light source [14, 18]. However, the light source here is assumed to be unpolarized and has an operating wavelength of 193 nm. Therefore, the discussion here does not consider either the pattern direction or the polarization. The repeated pattern is assumed to be fabricated using Cr on a SiO_2 mask plate. In the simulation, the pattern is defined as the single cycle shown in Figure 1, but it is repeated virtually to produce an infinite line-and-space pattern. The optical distribution near the mask is simulated by the finite-difference time-domain method. The aerial image at a distance from the mask is simulated by a method based on Fourier optics theory. The gap between the mask and the wafer can be regarded as being defocused from the Fourier imaging plane. The self-imaging point of the Talbot effect appears to correspond to the focusing point of the imaging optics. In proximity lithography, the mask pattern is transferred to the wafer surface at a gap from the mask. This gap offset is used for defocusing in projection optics. The lithographic tolerance is shown as a relationship between the exposure latitude and the gap offset variation for pattern width variation [19].

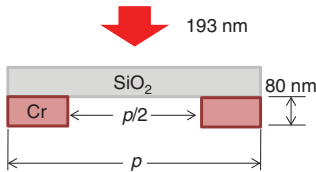


Figure 1: Mask pattern assumed for simulation. The mask has a repeated pattern formed in Cr on a SiO_2 mask plate.

The self-imaging point is repeated along the direction of light transmission at points separated by the Talbot distance. The Talbot distance, Z_T , is expressed as [2, 14]:

$$Z_T = \frac{2p^2}{\lambda}, \quad 2\lambda < p, \quad (1)$$

or

$$Z_T = \frac{p^2}{\lambda} \left(1 + \sqrt{1 - \left(\frac{\lambda}{p} \right)^2} \right), \quad p \approx \lambda, \quad (2)$$

where p is the pattern pitch, and λ is the wavelength of the light source.

3 Simulation results

In Figure 2A–C, the aerial images under the mask are shown at distances that range from one half to one and a half times the Talbot distance for each pattern pitch of (a) 230 nm, (b) 460 nm, and (c) 920 nm. The mask is illuminated through optics with a numerical aperture (NA) of 0.0002, which means that the light source is simply an untreated laser beam. In all cases, self-imaging appeared at the Talbot distance, and reversed images appeared at a distance of $\pm 0.5Z_T$ away from the Z_T point. The pitch size of 230 nm shown in Figure 2A is $< 2\lambda$. For this pattern size, the interference at the first Talbot distance is generated by only three waves from the neighboring secondary sources of the center aperture on the mask and the mask sides. If the pitch size is increased from 2λ to 3λ , then the interference at the first Talbot distance is generated by five waves,

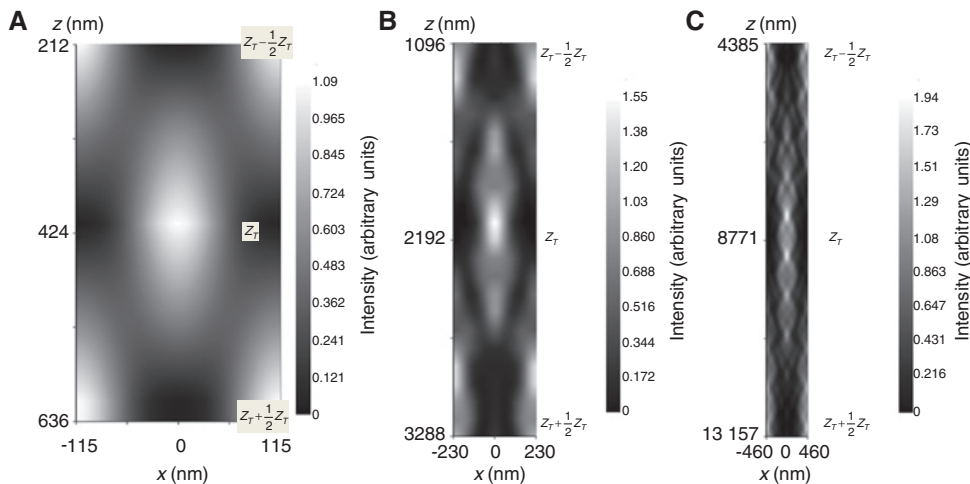


Figure 2: Aerial images under the mask shown at distances ranging from half to one and a half times the Talbot distance for each pattern pitch of (A) 230 nm, (B) 460 nm, and (C) 920 nm. The mask is illuminated using optics with a numerical aperture (NA) of 0.0002.

including the next neighboring waves. In this way, the self-imaging patterns with pitches of 230 nm, 460 nm, and 920 nm are composed of three waves, five waves, and nine waves, respectively. More waves are included as the pitch increases, and this leads to greater interference complexity. From a lithographic viewpoint, multiple fringe patterns caused by complex interference along the z -axis are not desirable because they lead to poor pattern fidelity tolerance of the gap variation between a mask and a wafer. A method is, therefore, required to remove this complex interference for increased process tolerance. During exposure, it is possible to average the image along the z -axis by moving the wafer stage. This method has previously been implemented in a projection tool [20]. Speckle in lithography, which is caused by use of a coherent source, has been also discussed [21]. This speckle is related to the interference of the coherent source. To reduce this interference, the coherent source must be changed until it is almost incoherent. The size of the source also has an influence on the interference.

Figure 3 shows aerial images of 920-nm-pitch line-and-space patterns produced using various illumination source sizes with NAs ranging from 0.01 to 0.05. The gray scale here matches that used in Figure 2C. As the NA of the illumination source increases, the interference fringes become less visible, while the image contrast simultaneously decreases, with values of 0.98 for a NA of 0.01, 0.95 for a NA of 0.02, 0.82 for a NA of 0.03, 0.57 for a NA of 0.04, and 0.29 for a NA of 0.05. To realize the effect of the source size on the pattern transfer characteristics, the

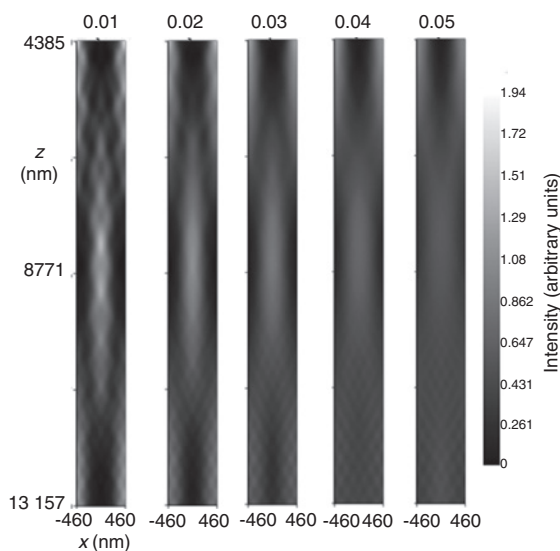


Figure 3: Aerial images of 920-nm-pitch line-and-space patterns with various illumination source sizes with NAs ranging from 0.01 to 0.05.

exposure-defocus (ED) tree of the aerial image is analyzed. Analysis of the ED tree is a useful method to ensure use of the appropriate exposure transfer tolerance and depth of focus (DOF), which is the depth of gap in this case [19, 22–26]. Figure 4 shows the intensity relative to the deviation of the gap from the Talbot distance for the linewidth of the 920-nm-pitch line-and-space pattern when the illumination source NA is 0.01. In this figure, the x -axis represents the intensity because the aerial image is simulated, but this intensity corresponds to the exposure dose applied to the resist. The three lines denote the exposure doses for -10%, nominal, and +10% varied linewidths. Using these lines, the process windows for the lithography process are obtained. The light blue square indicates the maximum window of the depth of gap at an exposure latitude of $\pm 10\%$ within a linewidth variation limit of $\pm 10\%$. The red square indicates the nominal window for that depth of gap. The nominal window includes both the so-called best focus and the best dose. In many cases, both in experiments or when processing send aheads, process windows are set based on this nominal window. In contrast, while the maximum window does not need to include the best dose, it offers no problems from a line width error perspective. The maximum window may be preferable, but many of the experiments are required to be performed at levels outside the range of the best

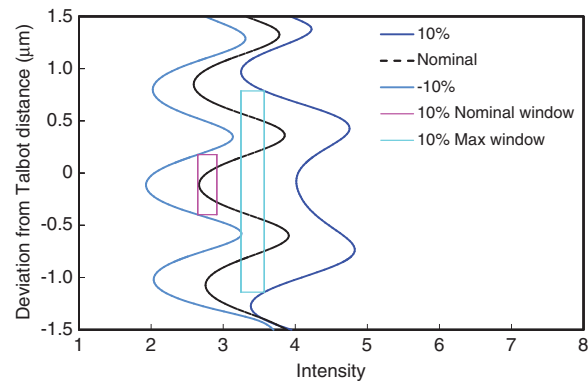


Figure 4: Intensity and deviation of the gap from the Talbot distance for the linewidth of the 920-nm-pitch line-and-space pattern when the illumination NA is 0.01. The x -axis represents the intensity because the aerial image is simulated, but this intensity corresponds to the exposure dose applied to the resist. The nominal window includes both the so-called best focus and the best dose. In many cases, both in experiments or when processing send aheads, process windows are set based on this nominal window. In contrast, while the maximum window does not need to include the best dose, it offers no problems from the line width error perspective. The maximum window may be preferable, but many of the experiments are required to be performed at levels outside the range of the best dose.

dose. If the exposure latitude criterion is changed, then the maximum and nominal DOFs will also change. The nominal DOF is smaller than the maximum DOF. Figure 5 shows the nominal and maximum DOFs for various illumination source NAs with 10% linewidth tolerance for the 920-nm-pitch line-and-space pattern. The nominal DOF for an illumination source with NA of 0.015 is 0.63 μm . If the illumination source is larger than that, then, the nominal DOF will be 1.83 μm at an illumination source NA of 0.03 or more. However, the nominal DOF is almost 0 μm when the illumination source NA is 0.05.

4 Discussion

The simulation results indicate that the appropriate illumination source NA should neither be too small nor too large. At the plane at the Talbot distance, the imaging pitch is the same as the original mask pattern pitch, p . The linewidth is $p/2$ under equal line-and-space pattern conditions. As mentioned in the previous section, the 920-nm-pitch pattern is composed of nine waves, which all have the same phase at the Talbot plane. However, outside the Talbot plane, these waves have different phases. This difference generates interference fringes, and then the imaging line is split. The width of the imaging line around the Talbot plane is approximately $p/2$. If the line is split into two lines, then, the new pitch for these two lines will be $p/4$. In the case where the line is split into more than two lines, the pitch of the new lines will be less than $p/4$. Therefore, the maximum split pitch is $p/4$, as shown in Figure 6A. Now, if a point light source is used, then, the interference will have ideal contrast. When the position of the source is gradually shifted, then, the interference

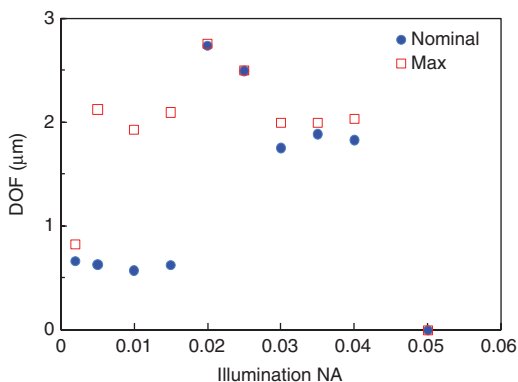


Figure 5: Nominal and maximum DOFs for various illumination NAs with 10% linewidth tolerance for the 920-nm-pitch line-and-space pattern.

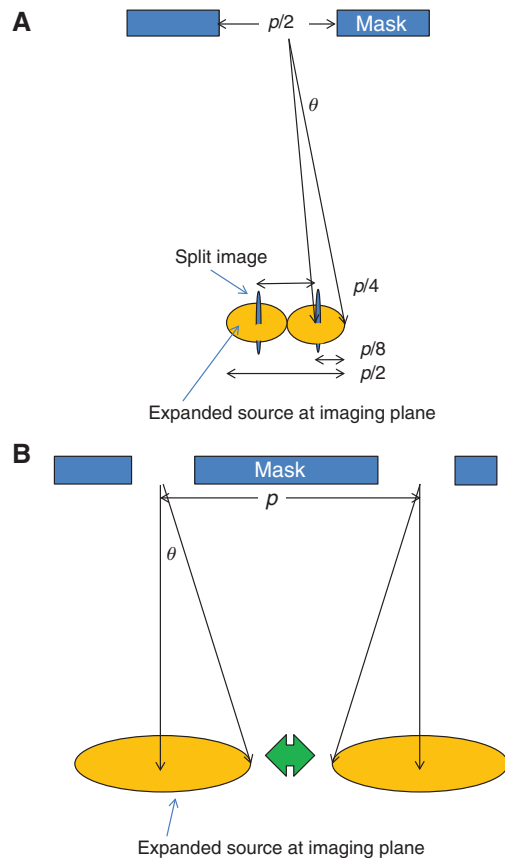


Figure 6: (A) Minimum illumination source size. (B) Maximum illumination source size.

fringe position will also be gradually shifted. Additionally, if the light source has an area, then, the interference fringe will also have an area that corresponds to that light source area. Here, the split fringes will be unified when each fringe is enlarged by the area light source. Those splits can, therefore, almost be made invisible by expanding the source to a radius of $p/8$. Under this condition, the space between the fringes is closed. This can be expressed as

$$\frac{p}{8} \leq Z_T \sin\theta \tag{3}$$

$$\leq \frac{2p^2}{\lambda} \sin\theta \tag{4}$$

Therefore, the following relationship is obtained:

$$\sin\theta \geq \frac{\lambda}{16p}. \tag{5}$$

The split subfringes are then erased when this expression is satisfied. The line in the imaged line-and-space pattern may be split into more than two parts. The source size required to make the split almost invisible is included

in the relationship of equation (5). However, the source will be limited to a maximum size. The pattern formed by the expanded source at the Talbot distance should not be allowed to overlap another neighboring pattern made by the expanded source, as shown in Figure 6B, so that high image contrast can be maintained. Figure 6B shows that the expanded source produces a pattern where the area corresponds to the source size and also shows that some space is required between these areas. This requirement can be expressed as:

$$\frac{p}{2} > Z_T \sin\theta \quad (6)$$

$$> \frac{2p^2}{\lambda} \sin\theta \quad (7)$$

Therefore, the following relationship is obtained:

$$\sin\theta < \frac{\lambda}{4p}. \quad (8)$$

Sufficient contrast is maintained by satisfying this expression. These expressions are valid only for small values of θ and low NAs. From the above discussion, the minimum and maximum conditions for the illumination source can be determined to be

$$\frac{\lambda}{16p} \leq \sin\theta < \frac{\lambda}{4p}. \quad (9)$$

This shows the appropriate region for the illumination source NA for use in submicron patterning by ArF Talbot lithography. The illumination source NA values that were obtained in the simulation results, where large process windows were shown, lie within in this region. This can, thus, be used as a guideline to determine the appropriate source size for Talbot lithography.

5 Conclusion

We investigated the effect on the DOF of the illumination source size based on interference patterns such as a Talbot carpet through simulations. In this study, submicron pattern transfer using a 193-nm ArF source was simulated. When the pattern pitch size was more than twice the wavelength, the Talbot carpet becomes complex, and many subfringe patterns appear because of interference. The appearance of the subfringes was related to the illumination source size. When a larger source size was applied, the subfringes became weaker. However, if the source size was so large as to overlap with the neighboring pattern

at the imaging plane, then, the image contrast would become very low. Therefore, to provide a large process window, a guideline to determine the appropriate source size was derived. We can select an appropriate source size using this guideline, and by suppressing the subfringes, a larger DOF for the process can be expected.

Acknowledgments: The authors would like to thank Satoshi Tanaka, Ryoichi Inanami, Kazuto Matsuki, and Shinichi Ito for fruitful discussions, and Tatsuhiko Higashiki and Shimon Maeda for providing management support. The authors also thank the Synopsys support team for their kind support of our simulation work.

References

- [1] H. F. Talbot, *Philos. Mag.* 9, 401 (1836).
- [2] L. Rayleigh, *Philos. Mag.* 11, 196 (1881).
- [3] J. Wen, Y. Zhang and M. Xiao, *Adv. Opt. Photon.* 5, 83 (2013).
- [4] C. Wagner and N. Harned, *Nature Photonics* 4.1, 24 (2010).
- [5] S. Mori, H. Aoyama, T. Ogata, R. Matsui and T. Matsuyama, *Proc. SPIE* 8683, 86830A (2013).
- [6] T. Higashiki, T. Nakasugi and I. Yoneda, *Proc. SPIE* 7970, 797003 (2011).
- [7] L. Stuerzebecher, F. Fuchs, U. D. Zeitner and A. Tuennermann, *Microelectron. Eng.* 132, 134 (2015).
- [8] C. Zanke, M. Qi and H. I. Smith, *J. Vac. Sci. Technol. B* 22, 3352 (2004).
- [9] A. Isoyan, F. Jiang, Y. C. Cheng, F. Cerrina, P. Wachulak, et al. *J. Vac. Sci. Technol. B* 27, 2931 (2009).
- [10] C. P. Fucetola, A. A. Patel, E. E. Moon, T. B. O'Reilly and H.I. Smith, *J. Vac. Sci. Technol. B* 27, 2947 (2009).
- [11] L. Stuerzebecher, T. Harzendorf, U. Vogler, U. D. Zeitner and R. Voelkel, *Opt. Express* 18, 19495 (2010).
- [12] H. H. Solak, C. Dais and F. Clube, *Opt. Express* 11, 10686 (2011).
- [13] L. Urbanski, W. Li, J. J. Rocca, C. S. Menoni, M. C. Marconi, et al. *J. Vac. Sci. Technol. B* 30, 06F502 (2012).
- [14] T. Sato, *J. Vac. Sci. Technol. B* 30, 06FG02 (2012).
- [15] S. Danylyuk, P. Loosen, K. Bergmann, H.-S. Kim and L. Juschkina, *J. Micro/Nanolith. MEMS MOEMS* 12, 033002 (2013).
- [16] T. Sato, *Microelectron. Eng.* 123, 80 (2014).
- [17] T. Sato, A. Yamada, T. Suto, R. Inanami, K. Matsuki, et al. *Microelectron. Eng.*, Available online 2 March 2015, ISSN 0167-9317,.
- [18] Y. Liu, C. Zhou, S. Wang and B. Wang, *J. Opt. Soc. Am. A* 23, 2154 (2006).
- [19] B. J. Lin, *J. Vac. Sci. Technol. B* 8, 1539 (1990).
- [20] H. Fukuda, N. Hasegawa, T. Tanaka and T. Hayashida, *Electron Device Lett. IEEE* 8, 179 (1987).
- [21] K. Jain and R. Kerth, *Appl. Opt.* 23, 648 (1984).
- [22] B. J. Lin, *IEEE Trans. Electron Devices* 27, 931(1980).
- [23] A. C. Liu, B. J. Lin, *IEEE Trans. Electron Devices* 30, 1251 (1983).
- [24] S. Nojima, S. Mimotogi, M. Itoh, O. Ikenaga, S. Hasebe, et al. *Proc. SPIE* 4754, 33 (2002).
- [25] S. Mimotogi, F. Uesawa, M. Tominaga, H. Fujise, K. Sho, et al. *Proc. SPIE* 6520, 652008 (2007).
- [26] D. Flagello and D. G. Smith, *Adv. Opt. Technol.* 1.4, 237 (2012).

Takashi Sato

Center for Semiconductor Research and Development, Toshiba Corporation 1, Komukai Toshiba-cho, Saiwai-ku, Kawasaki, Kanagawa 212-8583, Japan,
ta.sato@toshiba.co.jp

Takashi Sato received his Master of Engineering (1984) and Doctor of Engineering (2007) degrees from Tokyo Institute of Technology. He joined Toshiba in 1984. He has worked on the development of optical lithography in areas such as resolution enhancement techniques, alignment systems, deep UV lithography processing, the influence of mask topography, and lithography monitoring and modeling. He was assigned to IBM East Fishkill for 3 years from 1993 to take part in DRAM development. Recently, he has focused on lithographic simulations for future technology development. His current interests include nano-scale control and the cost effectiveness of lithography processes.

Akiko Yamada

Center for Semiconductor Research and Development, Toshiba Corporation 1, Komukai Toshiba-cho, Saiwai-ku, Kawasaki, Kanagawa 212-8583, Japan

Akiko Yamada received her Master of Science (1991) degree from Tokyo Metropolitan University. She joined Toshiba in 1991 and has worked in the lithographic processing field. She has optimized various process parameters, including antireflection and resist processing parameters. She has also been engaged in the development of DUV lithography, with specific contributions to resist development and process window analysis. She is currently working on process window prediction through lithographic simulations.

Takeshi Suto

Center for Semiconductor Research and Development, Toshiba Corporation 1, Komukai Toshiba-cho, Saiwai-ku, Kawasaki, Kanagawa 212-8583, Japan

Takeshi Suto joined Toshiba in 1991. He has worked on the development of lithography processes. He is currently engaged in lithography simulation work.